Resonance Raman Spectroscopic Core-Size Correlations for the Crystallographically Defined Complexes Fe^{II}(OEP), Fe^{II}(OEC), Fe^{III}(OEP)(NCS), $[Fe^{III}(OEP)(N\text{-MeIm})_2]^+$, and $[Fe^{III}(OEP)(DMSO)_2]^+$

Muthusamy Mylrajan,[1a,b] Laura A. Andersson,[1a,c] Jie Sun,[1a] Thomas M. Loehr,*[,1a] Carol S. Thomas,[1d,e] Eric P. Sullivan, Jr.,[1d] Mark A. Thomson,[1d] Kim M. Long,[1d] Oren P. Anderson,[1d] and Steven H. Strauss*[,1d]

Department of Chemistry, Biochemistry, and Molecular Biology, Oregon Graduate Institute of Science & Technology, Portland, Oregon 97291-1000, Department of Chemistry, Colorado State University, Fort Collins, Colorado 80523, and Department of Biochemistry, Kansas State University, Manhattan, Kansas 66506

Received January 20, 1995[⊗]

Resonance Raman (rR) spectroscopy of metalloporphyrins can provide detailed information about the oxidation state, coordination number, and spin state of the central metal ion. These data have been of particular value in the study of natural and model heme systems. Core-size correlations, plots of the porphyrin-ring center to pyrrole nitrogen (Ct−N) distances versus rR frequencies, are frequently utilized to assess structural properties or to confirm spectral assignments. However, in most cases, such plots for β-pyrrole-substituted porphyrins are limited by the use of Ct−N distances derived from the crystal structures of *meso*-tetraphenylporphyrins. Because of well-documented structural and spectroscopic differences in these two classes of porphyrins, the utility of such core-size correlations may be impaired. Here we report the crystal structures of three new octaethylporphyrin (OEP) complexes: (1) Fe(OEP)(NCS)·C_7H_8, triclinic, $P\bar{1}$, a = 11.669(2) Å, b = 12.151(2) Å, c = 14.251(3) Å, α = 73.77(1)°, β = 87.41(1)°, γ = 82.07(1)°, Z = 2, T = −130(1) °C; (2) $[Fe(OEP)(N\text{-MeIm})_2][Ag(N\text{-MeIm})_2][PF_6]_2$, $P\bar{1}$, a = 10.577(2) Å, b = 11.322(2) Å, c = 13.205(2) Å, α = 66.61(2)°, β = 82.43(2)°, γ = 77.51(2)°, Z = 1, T = −100(1)°C; (3) $[Fe(OEP)(DMSO)_2][PF_6]$, monoclinic, $C2/c$, a = 21.877(4) Å, b = 14.680(3) Å, c = 14.593(3) Å, β = 93.43(3)°, Z = 4, T = −100(1) °C. These three constitute a set of ferric compounds that are a high-spin pentacoordinate, a low-spin hexacoordinate, and a high-spin hexacoordinate, respectively. The rR properties of these three compounds together with rR data of two crystallographically defined intermediate-spin, tetracoordinate ferrous complexes, Fe(OEP) and Fe(OEC), are presented. The latter is a chlorin, i.e., a dihydroporphyrin, complex. The present rR data for these *crystallographically characterized complexes* permit the first rigorous test of earlier Ct−N vs ν correlations in that the spectroscopic and structural parameters are from the same compounds in the same crystalline phase and yield a new core-size correlation for β-pyrrole-substituted metalloporphyrins. With the present analysis as a foundation, rR spectroscopic studies may be extended to simple complexes in solution as well as heme proteins in the determination of core sizes and in facilitating spectral assignments.

Introduction

The oxidation state, coordination number, and spin state of iron(II,III) porphyrins are known to affect the equilibrium position of the metal ion with respect to the heme plane. These properties are important determinants for the chemical, functional, and mechanistic properties of heme proteins. Since the mid 1970s, resonance Raman (rR) frequencies have been noted to be sensitive to the relative location of the metal ion in metalloporphyrin complexes. The frequency of an anomalously polarized vibrational mode (~1550−1590 cm^{-1}, now known as ν_{19}) was the first rR spectral feature observed to reflect the in-plane or out-of-plane disposition of the metal ion.[2] This frequency was later found to obey an empirical correlation with the core size of the porphyrin, Ct−N, the measure of the center of the porphyrin ring to the pyrrole nitrogen atoms.[3] Later workers noted that ν_3 (~1470−1510 cm^{-1}) and ν_{10} (~1605−1660 cm^{-1}), both having significant C_a-C_m bond stretching contributions in their normal modes, also satisfied the core-size correlation.[4,5] Huong and Pommier[4] showed that the ν_{10} and ν_{19} frequencies of many metalloporphyrins followed a linear correlation with the Ct−N distance, d (in Å), such that $\nu = K(A-d)$.

Metalloporphyrins made nonplanar by ruffling and doming were shown to have markedly lower frequencies than predicted by such plots. The decreased C_a-C_m stretching force constants were attributed to a loss of π conjugation at the methine bridge carbons.[5] By including the methine-bridge dihedral angle, these workers satisfactorily modified the frequency vs core-size equation. Choi et al.[6] then showed that *all* porphyrin skeletal modes >1450 cm^{-1} (ν_{28}, ν_{38}, ν_{11}, ν_2, and ν_{37} in addition to ν_3, ν_{19}, and ν_{10}) exhibited negative correlations with the core size; the exact slopes vary with the normal mode composition of the particular frequency but extend to both C_a-C_m and C_b-C_b

⊗ Abstract published in *Advance ACS Abstracts,* June 15, 1995.

(1) (a) Oregon Graduate Institute of Science & Technology. (b) Current address: Regional Sophisticated Instrumentation Center, Indian Institute of Technology, Madras 600036, India. (c) Kansas State University. (d) Colorado State University. (e) Formerly Carol S. Harris.

(2) Felton, R. H.; Yu, N.-T.; OShea, D. C.; Shelnutt, J. A. *J. Am. Chem. Soc.* **1974**, *96*, 3675.

(3) Spaulding, L. D.; Chang, C. C.; Yu, N.-T.; Felton, R. H. *J. Am. Chem. Soc.* **1975**, *97*, 2517.

(4) Huong, P. V.; Pommier, J.-C. *C. R. Acad. Sci., Ser. C* **1977**, *285*, 519.

(5) Spiro, T. G.; Stong, J. D.; Stein, P. *J. Am. Chem. Soc.* **1979**, *101*, 2648.

(6) Choi, S.; Spiro, T. G.; Langry, K. C.; Smith, K. M.; Budd, L. D.; La Mar, G. N. *J. Am. Chem. Soc.* **1982**, *104*, 4345.

0020-1669/95/1334-3953$09.00/0

modes. This interesting development now makes it possible to *calculate* the expected position of rR modes in metalloporphyrins and heme systems (for the weaker or less-well-defined features) from a knowledge of a few readily apparent rR frequencies. Some investigators are, in fact, basing spectral assignments on such interpretations.

The applicability of core-size/frequency plots to metallochlorin complexes was first investigated by Andersson et al.,[7] who noted no clear-cut correlation between rR frequencies and expected core sizes of *meso*-substituted metallochlorins. However, Ozaki et al.,[8] in their study of metallooctaethylchlorins, M(OEC), observed linear correlations for rR frequencies vs extrapolated core sizes. Thus, although chlorins are distinct from the corresponding porphyrins in their specific normal-mode compositions,[9] their rR spectra still properly reflect structural parameters. Hence, they serve as diagnostic indicators for the spin and coordination state of the metal ion in the chlorin chromophore as previously found and reported.[10a-e] The caveat is that rR modes of hydroporphyrins must not be directly equated with porphyrin modes of similar frequencies; rather, the terms "porphyrin-equivalent" or "porphyrin-related" modes should be applied. Moreover, direct comparisons between porphyrin and chlorin frequencies are made difficult by the inherently greater complexity of hydroporphyrin rR spectra.[11,12]

Parthasarathi et al.[13] added the oxidation state marker ν_4 to the group of core-size-sensitive rR modes and presented revised coefficients for protoporphyrin and tetraphenylporphyrin (TPP)[14] complexes. Oertling and co-workers extended the study to porphyrin π-cation radicals and showed that the loss of an electron had only minor effects on the core-size/frequency correlations.[15] For the majority of these correlation studies, however, *the true core size of the macrocycle being studied by rR spectroscopy is not available from crystal data.* That is, the Ct−N distances used in the graphs for porphyrin and chlorin complexes were, in general, not for the macrocycle being studied, but based on those for the more readily available M(TPP) crystal data. The only exceptions are the well-studied Ni(OEP) complexes.[3,14,16-18]

In view of this situation, we have reinvestigated frequency/core-size correlations using *true* Ct−N distances. We report the crystal structures and resonance Raman properties of three new Fe^{III}(OEP) complexes: five-coordinate Fe(OEP)(NCS), six-coordinate $[Fe(OEP)(N\text{-MeIm})_2]^+$, and six-coordinate $[Fe(OEP)(DMSO)_2]^+$. In addition, we have investigated the vibrational spectra of Fe(OEP) and Fe(OEC), the only structurally characterized four-coordinate β-pyrrole-substituted Fe^{II} porphyrins and chlorins.[19] Although several rR and infrared (IR) studies of five- and six-coordinate Fe^{II}− and Fe^{III}−OEX (X = P or C) complexes have been reported,[5,8,20-24] no detailed rR and IR analyses of crystallographically defined four-coordinate Fe(OEX) complexes have appeared. However, a brief analysis of Fe(OEP) as a potential model for putative intermediate-spin heme proteins has been described.[25] With several new M(OEP) crystal structures, and hence reliable Ct−N distances, we present here a new frequency/core size correlation that is based on rR measurements of crystalline compounds of defined structure.

Experimental Section

Preparation of Compounds. All of the compounds in this study were air-sensitive to varying degrees and were handled using standard Schlenk and glovebox techniques.[26] The following reagents and solvents were obtained from Aldrich Chemical Co. and were either used as received or purified as follows: silver(I) hexafluorophosphate (used as received); dimethyl sulfoxide (DMSO, used as received); chlorobenzene (distilled from 4 Å molecular sieves); dichloromethane (distilled from P_2O_5); *N*-methylimidazole (*N*-MeIm; distilled from 4 Å molecular sieves); hexanes (distilled from sodium); toluene (distilled from sodium). The compounds Fe(OEP)Cl,[27] $[Fe(OEP)]_2O$,[28] Fe(OEP),[19c] and Fe(OEC)[19c] were prepared by literature procedures. The compound Fe(OEP)(NCS) was prepared by stirring a dichloromethane solution of $[Fe(OEP)]_2O$ with a large excess of 0.1 M aqueous solution of KNCS/$HClO_4$. The dichloromethane layer was placed under vacuum until a dry solid residue of Fe(OEP)(NCS) remained. Crystals of Fe(OEP)(NCS)·C_7H_8 were grown from a toluene solution. The compound $[Fe(OEP)(N\text{-MeIm})_2][Ag(N\text{-MeIm})_2][PF_6]_2$ was prepared and crystallized by treating Fe(OEP)Cl (0.028 g; 0.04 mmol) with $AgPF_6$ (0.020 g; 0.08 mmol) and *N*-MeIm (0.11 mL; 1.3 mmol) in several milliliters of chlorobenzene. After the white precipitate of AgCl was filtered off, the remaining solution was placed in a small glass vial, which in turn was placed in a larger, tightly capped vial containing hexanes. After several days, dark reddish-purple needle-shaped crystals were present. The compound $[Fe(OEP)(DMSO)_2][PF_6]$ was prepared and crystallized by treating Fe(OEP)Cl (0.028 g; 0.04 mmol) with $AgPF_6$ (0.020 g; 0.08 mmol) and DMSO (0.10 mL; 1.4 mmol) in several milliliters of chlorobenzene. After the white precipitate of AgCl was filtered off,

(7) Andersson, L. A.; Loehr, T. M.; Sotiriou, C.; Wu, W.; Chang, C. K. *J. Am. Chem. Soc.* **1986**, *108*, 2908.
(8) Ozaki, Y.; Iriyama, K.; Ogoshi, H.; Ochiai, T.; Kitagawa, T. *J. Phys. Chem.* **1986**, *90*, 6105.
(9) Boldt, N. J.; Donohoe, R. J.; Birge, R. R.; Bocian, D. F. *J. Am. Chem. Soc.* **1987**, *109*, 2284.
(10) (a) Andersson, L. A.; Loehr, T. M.; Lim, A. R.; Mauk, A. G. *J. Biol. Chem.* **1984**, *259*, 15340. (b) Andersson, L. A.; Loehr, T. M.; Chang, C. K.; Mauk, A. G. *J. Am. Chem. Soc.* **1985**, *107*, 182. (c) Andersson, L. A. *Proc. SPIE-Int. Soc. Opt. Eng.* **1989**, *1055*, 279. (d) Andersson, L. A.; Loehr, T. M.; Thompson, R. G.; Strauss, S. H. *Inorg. Chem.* **1990**, *29*, 2142. (e) Andersson, L. A.; Loehr, T. M.; Stershic, M. T.; Stolzenberg, A. M. *Inorg. Chem.* **1990**, *29*, 2278.
(11) Andersson, L. A.; Mylrajan, M.; Loehr, T. M.; Sullivan, E. P., Jr.; Strauss, S. H. *New J. Chem.* **1992**, *16*, 569.
(12) Andersson, L. A.; Mylrajan, M.; Loehr, T. M.; Chang, C. K. *Spectrochim. Acta* **1993**, *49A*, 2105.
(13) Parthasarathi, N.; Hansen, C.; Yamaguchi, S.; Spiro, T. G. *J. Am. Chem. Soc.* **1987**, *109*, 3865.
(14) OEP = 2,3,7,8,12,13,17,18-octaethylporphyrinate dianion; OEC = 7,8-dihydro-2,3,7,8,12,13,17,18-octaethylporphyrinate dianion (octaethylchlorinate dianion). OEX = generic name referring to either or both macrocyles. TPP = 5,10,15,20-tetraphenylporphyrinate dianion. PPIX = the dianion of protoporphyrin-IX (2,7,12,18-tetramethyl-3,8-divinylporphyrin-13,17-dipropionic acid); PPIXDME = the dimethyl ester of PPIX; PPIX−H = singly deprotonated PPIX.
(15) Oertling, W. A.; Salehi, A.; Chung, Y. C.; Leroi, G. E.; Chang, C. K.; Babcock, G. T. *J. Phys. Chem.* **1987**, *91*, 5887.
(16) Brennan, T. D.; Scheidt, W. R.; Shelnutt, J. A. J. *Am. Chem. Soc.* **1988**, *110*, 3919.
(17) (a) Cullen, D. L.; Meyer, E. F., Jr. *J. Am. Chem. Soc.* **1974**, *96*, 2095. (b) Meyer, E. F., Jr. *Acta Crystallogr.* **1972**, *B28*, 2162.
(18) Czernuszewicz, R. S.; Li, X.; Spiro, T. G. *J. Am. Chem. Soc.* **1989**, *111*, 7024.
(19) (a) Strauss, S. H.; Silver, M. E.; Ibers, J. A. *J. Am. Chem. Soc.* **1983**, *105*, 4108. (b) The four-coordinate Fe^{II}(tetraphenylporphyrin) is also structurally characterized: Collman, J. P.; Hoard, J. L.; Kim, N.; Lang, G.; Reed, C. A. *J. Am. Chem. Soc.* **1975**, *97*, 2676. (c) Strauss, S. H.; Silver, M. E.; Long, K. M.; Thompson, R. G.; Hudgens, R. A.; Spartalian, K.; Ibers, J. A. *J. Am. Chem. Soc.* **1985**, *107*, 4207.
(20) Ogoshi, H.; Watanabe, E.; Yoshida, Z.; Kincaid, J. R.; Nakamoto, K. *J. Am. Chem. Soc.* **1973**, *95*, 2845.
(21) (a) Kitagawa, T.; Ogoshi, H.; Watanabe, E.; Yoshida, Z. *J. Phys. Chem.* **1975**, *79*, 2629. (b) Kitagawa, T.; Abe, M.; Kyogoku, Y.; Ogoshi, H.; Watanabe, E.; Yoshida, Z. *J. Phys. Chem.* **1976**, *80*, 1181. (c) Kitagawa, T.; Abe, M.; Ogoshi, H. *J. Chem. Phys.* **1978**, *69*, 4516.
(22) Ozaki, Y.; Kitagawa, T.; Ogoshi, H. *Inorg. Chem.* **1979**, *18*, 1772.
(23) Choi, S.; Spiro, T. G. *J. Am. Chem. Soc.* **1983**, *105*, 3683.
(24) Boldt, N. J.; Bocian, D. F. *J. Phys. Chem.* **1988**, *92*, 581.
(25) Andersson, L. A.; Mylrajan, M.; Sullivan, E. P., Jr.; Strauss, S. H. *J. Biol. Chem.* **1989**, *264*, 19099.
(26) (a) Wayda, A. L.; Darensbourg, M. Y. *Experimental Organometallic Chemistry*; American Chemical Society: Washington, DC, 1987. (b) Shriver, D. F.; Drezdzon, M. A. *The Manipulation of Air−Sensitive Compounds*, 2nd ed.; Wiley-Interscience: New York, 1986.
(27) Adler, A. D.; Longo, F. R.; Varadi, V. *Inorg. Synth.* **1976**, *16*, 213.
(28) Buchler, J. W.; Schneehage, H. H. *Z. Naturforsch., B: Anorg. Chem., Org. Chem.* **1973**, *28B*, 433.

Table 1. Details of the X-ray Diffraction Studies of Fe(OEP)(NCS)·C_7H_8, [Fe(OEP)(*N*-MeIm)$_2$][Ag(*N*-MeIm)$_2$][PF_6]$_2$, and [Fe(OEP)(DMSO)$_2$][PF_6]

compd	Fe(OEP)(NCS)·C_7H_8	[Fe(OEP)(*N*-MeIm)$_2$][Ag(*N*-MeIm)$_2$][PF_6]$_2$	[Fe(OEP)(DMSO)$_2$][PF_6]
molecular formula	$C_{44}H_{52}FeN_5S$	$C_{52}H_{68}AgF_{12}FeN_{12}P_2$	$C_{40}H_{56}F_6FeN_4O_2PS_2$
fw	738.8	1314.8	889.8
space group	$P\bar{1}$	$P\bar{1}$	$C2/c$
unit cell dimens			
a, Å	11.669(2)	10.577(2)	21.877(4)
b, Å	12.151(2)	11.322(2)	14.680(3)
c, Å	14.251(3)	13.205(2)	14.593(3)
α, deg	73.77(1)	66.61(2)	90
β, deg	87.41(1)	82.43(2)	93.43(3)
γ, deg	82.07(1)	77.51(2)	90
unit cell vol, Å^3	1921.5(4)	1415.2(4)	4678(2)
Z	2	1	4
calcd density, g cm^{-3}	1.28	1.54	1.26
cryst dimens, mm	0.20 × 0.36 × 0.54	0.42 × 0.42 × 0.28	0.12 × 0.12 × 0.12
data collcn temp, °C	−130(1)	−100(1)	−100(1)
radiation (λ, Å)	Mo Kα (0.7107)	Mo Kα (0.7107)	Mo Kα (0.7107)
monochromator	graphite	graphite	graphite
abs coeff, cm^{-1}	4.79	7.46	5.15
scan type	θ−2θ	θ−2θ	θ−2θ
scan speed, deg min^{-1}	variable (2−30)	variable (4−30)	variable (4−30)
2θ range, deg	4−50	4−50	4−50
reflcns	$\pm h,\pm k,-l$	$\pm h,\pm k,-l$	$\pm h,k,l$
tot. no. of reflcns measd	7066	5229	4324
no. of obsd reflcns			
$\|F_o\| > 4.0\sigma(F_o)$	5680		
$\|F_o\| > 2.5\sigma(F_o)$		4450	2818
data/param ratio	11.7	12.2	11.1
R	0.039	0.038	0.097
R_w	0.052	0.054	0.144
GOF	1.58	1.48	0.97
g (refined)	0.00057	0.0008	0.0157

the remaining solution was placed in one arm of an "h"-shaped glass tube equipped with a Teflon valve. The other arm contained hexanes. After several weeks, dark reddish-purple needle-shaped crystals were present.

Crystallographic Studies. For the three compounds, Fe(OEP)(NCS)·C_7H_8, [Fe(OEP)(*N*-MeIm)$_2$][Ag(*N*-MeIm)$_2$][PF_6]$_2$, and [Fe(OEP)(DMSO)$_2$][PF_6], centering of 25 reflections on a Siemens *R3m* diffractometer allowed least-squares calculation of the cell constants listed in Table 1. Other experimental parameters are also listed in Table 1. For Fe(OEP)(NCS)·C_7H_8, the intensities of three control reflections ($\bar{5}\bar{1}\bar{4}$, $\bar{1}3\bar{5}$, $\bar{4}2\bar{4}$) monitored every 197 reflections showed no significant change in intensity during the course of the data collection. For [Fe(OEP)(*N*-MeIm)$_2$][Ag(*N*-MeIm)$_2$][PF_6]$_2$ and [Fe(OEP)(DMSO)$_2$][PF_6], the intensities of three control reflections (200, 020, 001 and 400, 020, 002, respectively) monitored every 97 reflections showed no significant change in intensity during the course of the data collection. Lorentz and polarization corrections were applied to all three sets of data. The structure of Fe(OEP)(NCS)·C_7H_8 was solved by using the direct methods program RANT.[29] The iron atoms in [Fe(OEP)(*N*-MeIm)$_2$][Ag(*N*-MeIm)$_2$][PF_6]$_2$ and [Fe(OEP)(DMSO)$_2$][PF_6] were located by Patterson methods and were found to occupy special positions, (0, y, $^1/_4$) and ($^1/_2$, 0, $^1/_2$), respectively. Coordinates for all other non-hydrogen atoms were determined from difference electron density maps. For all three structures, neutral-atom scattering factors with anomalous scattering contributions were employed,[30] and hydrogen atoms were included in calculated positions (C−H = 0.96 Å, U(H) = 1.2U_{iso}(C)). In the final difference Fourier synthesis, the maximum and minimum electron densities were 0.62 and −0.29 e Å^{-3} for Fe(OEP)(NCS)·C_7H_8, 0.50 and −0.67 e Å^{-3} for [Fe(OEP)(*N*-MeIm)$_2$][Ag(*N*-MeIm)$_2$][PF_6]$_2$, and 2.36 and −0.55 e Å^{-3} for [Fe(OEP)(DMSO)$_2$][PF_6]. Selected bond distances and angles are listed in Table 2. Complete tables of atomic coordinates, bond distances and angles, anisotropic thermal parameters for non-hydrogen atoms, and hydrogen atom coordinates are available as supporting information.

Spectroscopy. Infrared spectra were obtained from anaerobically prepared samples in Fluorolube and/or Nujol mulls on a Perkin-Elmer 983 spectrophotometer. Raman spectra were collected with computer-controlled scanning spectrophotometers: Dilor Z24 and Jarrell-Ash 25-300. All data analyses were carried out with our own data reduction procedures as previously reported.[31] Spectra Physics 164-05 (Ar), 2025-11 (Kr), and Coherent INNOVA 90-6 (Ar) lasers and a Coherent 599-01 dye laser (rhodamine 6G) served as excitation sources. Resonance Raman spectra of the Fe^{II} complexes were obtained both from pure solid samples in sealed capillaries and from solution samples in C_6H_6 and C_6D_6 sealed in NMR tubes. The samples were maintained at ~280 K by placing the sample tube into a copper or aluminum cold-finger immersed in a Dewar filled with an ice/water mixture. Low-temperature (~90 K) measurements were performed by filling the Dewar vessel with liquid nitrogen. For the Fe^{III} complexes, rR spectra were obtained from spinning samples made from pure solids diluted with KBr (1 mg: 200 mg KBr) or Na_2SO_4 (1−3% w/w) and were illuminated in a backscattering geometry. Polarization measurements were carried out with an analyzer and a polarization scrambler. Standard depolarization ratios of CCl_4 were checked for each wavelength. Frequencies were calibrated against indene (IUPAC standard).

Results and Discussion

Structure of Fe(OEP)(NCS)·C_7H_8. As has been found for the vast majority of four- and five-coordinate metal complexes of octaethylporphyrin,[32] pairs of Fe(OEP)(NCS) molecules exist as $\pi-\pi$ dimers in the solid state (the two halves of the [Fe(OEP)(NCS)]$_2$ dimers are related by a center of inversion).[33]

(29) All structural calculations were performed with the SHELXTL program library written by G. M. Sheldrick and supplied by Siemens Analytical X-Ray Instruments, Inc., Madison, WI.

(30) *International Tables for X-Ray Crystallography*; Kynoch: Birmingham, U. K., 1974; Vol. IV.

(31) (a) Loehr, T. M.; Keyes, W. E.; Pincus, P. A. *Anal. Biochem.* **1979**, *96*, 456. (b) The computer has been upgraded to an RMX286/Intel 310 system running our own revised Fortran 77 spectral data analysis programs. Figures 11 and 12 were plotted with LabCalc from Galactic Industries Corp., Salem, NH.

(32) Scheidt, W. R.; Lee, Y. J. *Struct. Bonding (Berlin)* **1987**, *64*, 1.

(33) Calculated values for parameters defined in ref 32 are: M.P.S. = 3.46; Ct−Ct = 4.813; Fe−Fe = 5.475; L.S. = 3.35; S.A.(Ct) = 44.0; S.A.(Fe) = 50.8. The two halves of the [Fe(OEP)(NCS)]$_2$ dimer are related by a center of inversion.

Table 2. Bond Distances (Å) and Angles (deg) for Fe(OEP)(NCS)•C_7H_8, [Fe(OEP)(*N*-MeIm)$_2$][Ag(*N*-MeIm)$_2$][PF_6]$_2$, [Fe(OEP)(DMSO)$_2$][PF_6], Fe(OEP), and Fe(OEC)[a]

	Fe(OEP)(NCS)•C_7H_8	[Fe(OEP)(*N*-MeIm)$_2$][Ag(*N*-MeIm)$_2$][PF_6]$_2$	[Fe(OEP)(DMSO)$_2$][PF_6]	Fe(OEP)[b]	Fe(OEC)[b]
Fe–N1	1.962(2)	2.003(2)	2.038(9)	1.984(5)	1.969(3)
Fe–N2	2.059(2)	2.005(2)	2.030(6)	2.007(5)	1.987(4)
Fe–N3	2.055(2)	1.975(2)	2.042(9)		2.002(4)
Fe–N4	2.058(2)				
Fe–N5	2.063(2)				
Fe–O			2.082(5)		
Ag–N		2.099(3)			
N1–C1	1.166(3)				
C–S	1.617(2)[c]		1.80(1)[d]		
C20–S			1.77(1)		
O–S			1.539(6)		
P–F		1.576(2)–1.608(2)	1.57(1)–1.59(1)		
N1–Fe–N2	100.5(1)	90.7(1)	90.0(2)		
N1–Fe–N3	103.3(1)	89.4(1)	180		
N1–Fe–N4	103.9(1)				
N1–Fe–N5	100.0(1)				
N2–Fe–N3	87.6(1)	89.3(1)	90.0(2)		
N2–Fe–N4	155.6(1)				
N2–Fe–N5	87.5(1)				
N3–Fe–N4	87.4(1)				
N3–Fe–N5	156.6(1)				
N4–Fe–N5	87.6(1)				
Fe–N1–C1	177.4(2)				
N1–C1–S	179.7(2)				
N5–Ag–N5′		180			
O–Fe–N1			90.6(2)		
O–Fe–N2			88.6(2)		
O–Fe–N3			89.4(2)		
O-Fe–O′			178.8(3)		
Fe–O–S			118.3(3)		
F–P–F(*cis*)		88.5(1)–91.7(1)	86.2(7)–93.8(7)		
F–P–F(*trans*)		177.8(2)–179.3(1)	180		

[a] All data from this work unless otherwise noted; OEP = 2,3,7,8,12,13,17,18-octaethylporphyrinate dianion; OEC = 7,8-dihydro-2,3,7,8,12,13,17,18-octaethylporphyrinate dianion (octaethylchlorinate dianion); Ct–N values and ligation/spin states of these complexes are given in Table 4. [b] Data from refs 19a and 19c. [c] C = C1. [d] C = C19.

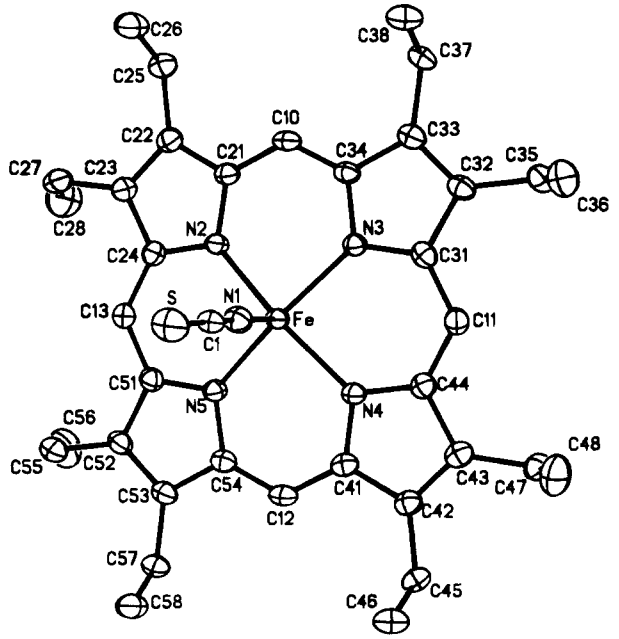

Figure 1. Structure of the Fe(OEP)(NCS) molecule (50% probability thermal ellipsoids). Hydrogen atoms have been omitted for clarity. The four N_p–Fe–N_l angles range from 100.0(1) to 103.9(1)°.

Figure 1 is a drawing of an individual Fe(OEP)(NCS) molecule. Figure 2 is a line drawing showing the average bond distances and angles for chemically equivalent structural units as well as the perpendicular displacement of each atom from the least-squares plane through the 24 atoms of the porphyrin core. It can be seen that the OEP core in this compound exhibits a quasi-C_{4v} doming distortion characteristic of five-coordinate metalloporphyrin complexes.[34]

On the basis of the structural results, the Fe(III) ion is evidently high-spin ($S = {}^5/_2$). The average Fe–N_{por} bond distance is 2.059(3) Å, which is similar to an average value of 2.069(8) Å found for a series of five-coordinate, high-spin Fe(III) porphyrin complexes[32] and the value of 2.048(4) Å reported for the six-coordinate high-spin complex Fe(OEP)(NCS)(pyridine).[35] The Fe–(NCS) bond distance of 1.962(2) Å is comparable to the 1.957(5) Å distance observed in five-coordinate high-spin Fe(TPP)(NCS)[14,36] but is shorter than the 2.031(2) Å distance observed in Fe(OEP)(NCS)(pyridine).[35] The perpendicular displacement of the iron atom from the least-squares planes of the four porphyrin nitrogen atoms and of the 24-atom porphyrin core are 0.426 and 0.481 Å, respectively. In the structure of Fe(PPIXDME)(*p*-$SC_6H_4NO_2$),[14] another five-coordinate high-spin Fe(III) porphyrin complex involving a related porphyrin with carbon-atom substituents at the 2, 3, 7, 8, 12, 13, 17, and 18 positions, the perpendicular displacements were found to be 0.434 and 0.448 Å, respectively (the average Fe–N_{por} bond distance was found to be 2.064(5) Å).[37] The

(34) (a) Scheidt, W. R.; Gouterman, M. In *Iron Porphyrins*; Lever, A. B. P., Gray, H. B., Eds.; Addison-Wesley: Reading, MA, 1983; Part I, p 89. (b) Scheidt, W. R.; Reed, C. A. *Chem. Rev.* **1981**, *81*, 543. (c) Hoard, J. L. In *Porphyrins and Metalloporphyrins*; Smith, K. M., Ed.; Elsevier: Amsterdam, 1975; Chapter 8.
(35) Scheidt, W. R.; Lee, Y. J.; Geiger, D. K.; Taylor, K.; Hatano, K. *J. Am. Chem. Soc.* **1982**, *104*, 3367.
(36) Bloom, A.; Hoard, J. L. *Abstracts of Papers*, 173rd National Meeting of the American Chemical Society, New Orleans, LA, March 1977; American Chemical Society: Washington, DC, 1977; INORG 27.
(37) Tang, S. C.; Koch, S.; Papaefthymiou, G. C.; Foner, S.; Frankel, R. B.; Ibers, J. A.; Holm, R. H. *J. Am. Chem. Soc.* **1976**, *98*, 2414.

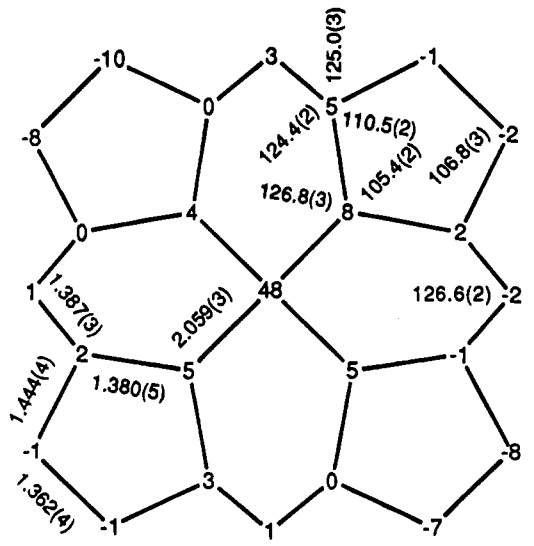

Figure 2. Diagram of the porphyrinato core of the Fe(OEP)(NCS) molecule displaying the perpendicular displacements (in units of 0.01 Å) of each atom from the least-squares plane through the 24-atom core. The average values of selected bonding parameters have been included. The orientation of the core is the same as that in Figure 1.

transannular N···N distances in Fe(OEP)(NCS)·C_7H_8 are 4.024 Å (N2···N4) and 4.033 Å (N3···N5), making the OEP core size (i.e., the average Ct−N separation) 2.014 Å in this compound (note that the definition of the N_4 center (Ct) is somewhat arbitrary since no symmetry is imposed on the N_4 unit).

Structure of [Fe(OEP)(*N*-MeIm)$_2$][Ag(*N*-MeIm)$_2$][PF_6]$_2$. This compound crystallized with one discrete six-coordinate [Fe(OEP)(*N*-MeIm)$_2$]$^+$ complex, one discrete two-coordinate [Ag(*N*-MeIm)$_2$]$^+$ complex, and two PF_6^- anions in the unit cell. Figure 3 is a drawing of the unit cell contents. Figure 4 is a line drawing showing the perpendicular displacement of each atom from the least-squares plane through the 24 atoms of the porphyrin core. The Fe(N_{por})$_4$ unit is rigorously planar, but the porphyrin core is distorted so that two adjacent pyrrole rings are slightly tilted up whereas the other two are slightly tilted down. The iron atom and the silver atom are both located on inversion centers. The Ag−N bond distance of 2.099(3) is similar to the Ag−N distances of 2.120(8) and 2.132(8) Å found in [Ag(Im)$_2$][NO_3].[38] As required by symmetry, the two planar *N*-MeIm ligands in the iron complex are coplanar. The dihedral angle formed between the *N*-MeIm plane and the nearest Fe−N_{por} vector is 20°. The analogous dihedral angles for [Fe(TPP)(*N*-MeIm)$_2$][ClO_4][39] and Fe(PPIX−H)(*N*-MeIm)$_2$·MeOH·H_2O[14,40] are 10 and 28°, respectively.

As expected for an Fe(III) porphyrin complex with relatively strong axial ligands,[34] the Fe(III) ion in the [Fe(OEP)(*N*-MeIm)$_2$]$^+$ complex is apparently low spin ($S = {}^1/_2$). The average Fe−N_{por} bond distance of 2.004(2) Å compares favorably with the average Fe−N_{por} distances of 1.982(3) and 1.991(5) Å for [Fe(TPP)(*N*-MeIm)$_2$][ClO_4][39] and Fe(PPIX−H)(*N*-MeIm)$_2$,[40] respectively. The Fe−N_{ax} bond distance of 1.975(2) Å is the same, to within experimental error, to the average Fe−N_{ax} distances of 1.974(3) and 1.977(5) Å for [Fe(TPP)(*N*-MeIm)$_2$][ClO_4] and Fe(PPIX−H)(*N*-MeIm)$_2$, respectively. Since the Fe(N_{por})$_4$ moiety in the [Fe(OEP)(*N*-MeIm)$_2$]$^+$ cation is rigorously planar, the OEP core size in this complex is equal to the average Fe−N_{por} bond distance, 2.004(2) Å.

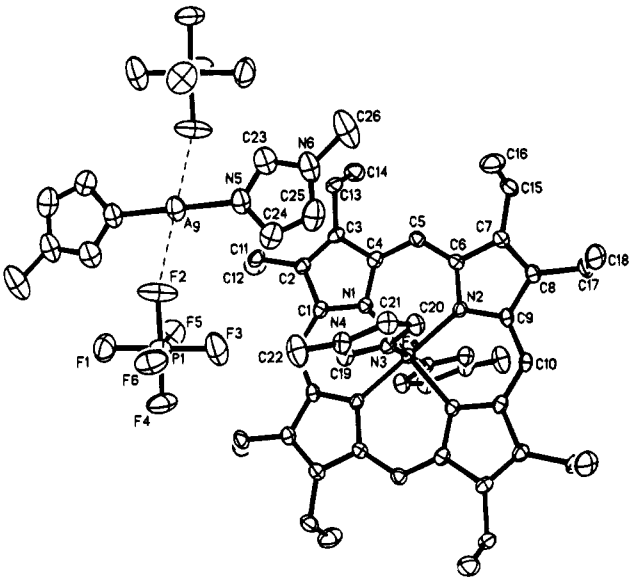

Figure 3. Structure of [Fe(OEP)(*N*-MeIm)$_2$][Ag(*N*-MeIm)$_2$][PF_6]$_2$ (50% probability thermal ellipsoids). Hydrogen atoms have been omitted for clarity. The separation of the various ions is to scale.

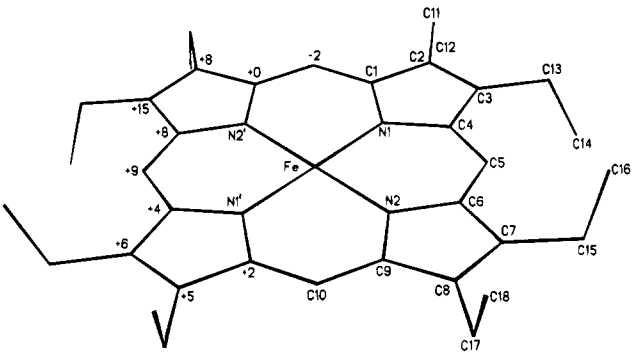

Figure 4. Drawing showing the perpendicular displacement of each atom from the least-squares plane through the 24 atoms of the porphyrin core of [Fe(OEP)(*N*-MeIm)$_2$][Ag(*N*-MeIm)$_2$][PF_6]$_2$. Although the Fe(N_{por})$_4$ unit is rigorously planar, the porphyrin core is distorted so that two adjacent pyrrole rings (left rear and left front) are slightly tilted up and two (right rear and right front) are slightly tilted down.

Structure of [Fe(OEP)(DMSO)$_2$][PF_6]. This compound crystallized with four [Fe(OEP)(DMSO)$_2$]$^+$ cations and four PF_6^- anions per unit cell. Each porphyrin complex is located on a crystallographic 2-fold axis that passes through the iron atom and the two porphyrin nitrogen atoms N1 and N3. The phosphorus atom is also located on a 2-fold axis. An obvious disorder of the pyrrole ring containing N3, involving the symmetry-related ethyl groups and the β-carbon atoms to which they are attached, was observed. The disorder was modeled by setting the unique β-carbon atom as a half-atom and allowing it to refine isotropically. This atom refined to two positions which defined the disordered pyrrole ring as either tilted up or down relative to the mean porphyrin plane. However, this model requires a nonplanar, twisted conformation for the disordered pyrrole ring, which is inconsistent with normal porphyrin stereochemistry. In addition, the modeling of the ethyl groups on the disordered pyrrole ring was not successful. The disorder is apparently more complex than a simple up or down positioning of the ethyl groups. The lack of a completely successful model for the disorder is indicated by the large value of *R* for this structure and by some unusual thermal parameters. Despite the disorder, the thermal parameters for the iron atom, the four nitrogen atoms, and the two oxygen atoms are entirely

(38) Antti, C.-J.; Lundberg, B. K. S. *Acta Chem. Scand.* **1971**, *25*, 1758.
(39) Higgins, T.; Safo, M. K.; Scheidt, W. R. *Inorg. Chim. Acta* **1991**, *178*, 261.
(40) Little, R. G.; Dymock, K. R.; Ibers, J. A. *J. Am. Chem. Soc.* **1975**, *97*, 4532.

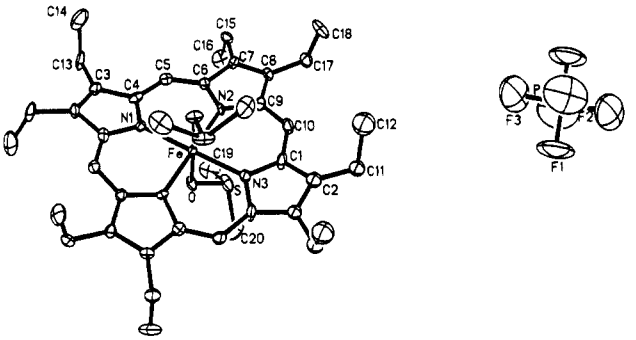

Figure 5. Structure of $[Fe(OEP)(DMSO)_2][PF_6]$ (50% probability thermal ellipsoids). Hydrogen atoms have been omitted for clarity. The separation of the ions is to scale.

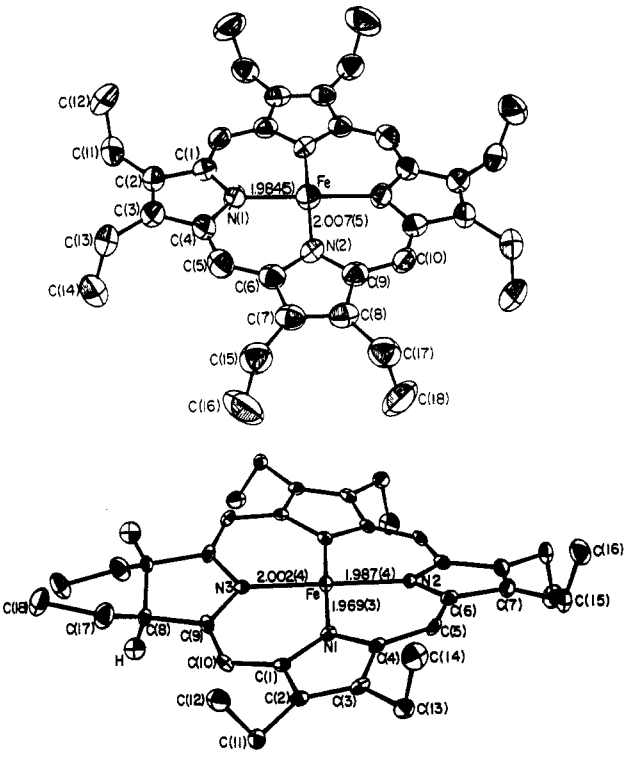

Figure 6. X-ray structures of the four-coordinate, divalent, intermediate spin ($S = 1$) Fe(OEP) and Fe(OEC) complexes (50% probability thermal ellipsoids), from refs 19a and 19c.

reasonable. Figure 5 is a drawing of the $[Fe(OEP)(DMSO)_2][PF_6]$ formula unit.

As expected for an Fe(III) porphyrin complex with relatively weak axial ligands,[34] the Fe(III) ion in the $[Fe(OEP)(DMSO)_2]^+$ complex is apparently high spin ($S = {}^5/_2$). The average Fe–N_{por} bond distance of 2.035(9) Å compares favorably with the average Fe–N_{por} distances of 2.045(5) and 2.045(8) Å for $[Fe(TPP)(TMSO)_2][ClO_4]$[41] (TMSO = tetramethylene sulfoxide) and $[Fe(TPP)(H_2O)_2][ClO_4]$,[42] respectively. In addition, the Fe–O distances in the $[Fe(OEP)(DMSO)_2]^+$ and $[Fe(TPP)(TMSO)_2]^+$ cations, 2.082(5) and 2.078(3) Å, respectively, are the same to within experimental error. Since the $Fe(N_{por})_4$ moiety in the $[Fe(OEP)(DMSO)_2]^+$ cation is rigorously planar, the OEP core size in this complex is equal to the average Fe–N_{por} bond distance, 2.035(9) Å.

Structures of Fe(OEP) and Fe(OEC). The preparation, characterization, and structural determinations of Fe(OEP) and Fe(OEC) have been reported.[19a,19c] Drawings of the structures are shown in Figure 6. Fe(OEP) belongs to a triclinic space group $P\bar{1}$ ($Z = 1$) and has a crystallographically imposed inversion center; its porphyrin ring is essentially planar, and its average Ct–N distance is 1.996(5) Å.[19c] Fe(OEC) exists in an orthorhombic space group *Pbcn* ($Z = 4$) and has C_2 site symmetry; the chlorin macrocycle is significantly S_4 ruffled even though the iron and the four nitrogens are rigorously coplanar.[19c] In Fe(OEC), the average Ct–N distance is 1.982(4) Å.[19c]

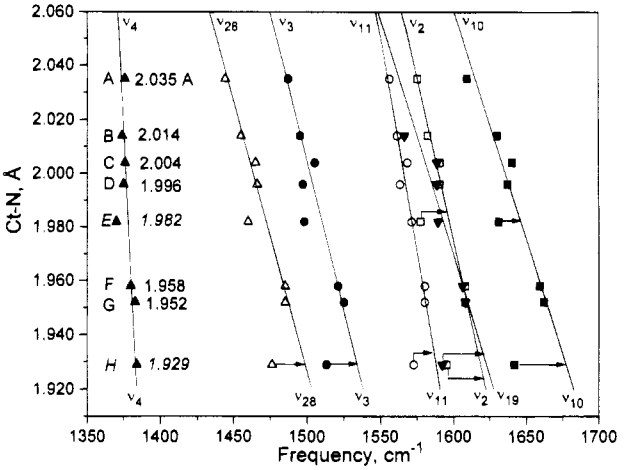

Figure 7. Core-size plot based on crystallographically defined structures: (A) $[Fe(OEP)(DMSO)_2][PF_6]$, $d = 2.035$ Å (this work); (B) Fe(OEP)(NCS), $d = 2.014$ Å (this work); (C) $[Fe(OEP)(N\text{-MeIm})_2][Ag(N\text{-MeIm})_2][PF_6]_2$, $d = 2.004$ Å (this work); (D) Fe(OEP), $d = 1.996$ Å (ref 19a); (E) Fe(OEC), $d = 1.982$ Å (ref 19c); (F) triclinic Ni(OEP), "A" form, $d = 1.958$ Å (refs 16 and 17a); (G) triclinic Ni(OEP), "B" form, $d = 1.952$ Å (refs 16 and 17a); (H) tetragonal Ni(OEP), $d = 1.929$ Å (ref 17b). The ruffled structures *E* and *H* were excluded from the linear least-squares fits. The calculated regression lines are based on the available frequency data for the crystalline iron complexes (Table 4) and the triclinic Ni complexes (refs 16 and 18).

Core-Size Correlations. (The discussion of individual rR spectra follows this section.) A plot of the core sizes versus rR frequencies using crystallographically determined Ct–N distances of the complexes reported here is shown in Figure 7. Included are data for the well-studied Ni(OEP) complexes.[3,16–18] This plot shows the trends of the vibrational modes ν_2, ν_3, ν_4, ν_{10}, ν_{11}, ν_{19}, and ν_{28} of these complexes as a function of core size. Complexes A, B, and C in Figure 7 are the three new Fe^{III} structures reported in this paper: $[Fe(OEP)(DMSO)_2]^+$, $[Fe(OEP)(N\text{-MeIm})_2]^+$, and Fe(OEP)(NCS), respectively. Complex D is Fe(OEP), the four-coordinate, intermediate-spin ferrous compound, and complex E is the corresponding hydroporphyrin, Fe(OEC). The remaining three entries are for Ni(OEP): complexes F and G are the triclinic forms *"A"* and *"B"*, respectively, of Ni(OEP) possessing D_{4h} symmetry,[16] and complex H is the tetragonal form of D_{2d} symmetry.[17] Complexes E and H, both of which are S_4-ruffled, were excluded in the least-squares fit to the data in the core-size plot. Deviations for domed and ruffled porphyrins have been discussed previously.[5,43] (For highly substituted, nonplanar porphyrins, the core-size/frequency correlations break down.[44])

The linear least-squares lines for the series of 6 complexes (A–D, F, and G) are quite satisfactory with the exception of

(41) Mashiko, T.; Kastner, M. E.; Spartalian, K.; Scheidt, W. R.; Reed, C. A. *J. Am. Chem. Soc.* **1978**, *100*, 6354.
(42) Scheidt, W. R.; Cohen, I. A.; Kastner, M. E. *Biochemistry* **1979**, *18*, 3546.
(43) Prendergast, K; Spiro, T. G. *J. Am. Chem. Soc.* **1992**, *114*, 3793.
(44) (a) Shelnutt, J. A.; Medforth, C. J.; Berber, M. D.; Barkigia, K. M.; Smith, K. M. *J. Am. Chem. Soc.* **1991**, *113*, 4077. (b) Shelnutt, J. A.; Majumder, S. A.; Sparks, L. D.; Hobbs, J. D.; Medforth, C. J.; Senge, M. O.; Smith, K. M.; Miura, M.; Luo, L.; Quirke, J. M. E. *J. Raman Spectrosc.* **1992**, *23*, 523.

Table 3. $M^{II,III}$(OEP) Resonance Raman Frequency/Core-Size Correlation Parameters from Crystallographically Defined Structures Compared with Literature Values

		this work[a]		ref 13[b]		ref 15[c]		ref 8[d]	
mode	description	*K*	*A*	*K*	*A*	*K*	*A*	*K*	*A*
ν_2	C_b-C_b (60%)	413.7	5.842	329.6	6.78	243	8.56	322.3	6.93
ν_3	C_a-C_m (41%)	452.2	5.321	423.7	5.53	383	5.93	413.8	5.63
ν_4	C_a-N (53%)	90.32	17.24	136.7	12.07				
ν_{10}	C_a-C_m (49%)	589.1	4.776	564.9	4.89	415	5.94	494.4	5.30
ν_{11}	C_b-C_b (57%)	310.6	7.040	353.1	6.42	197	9.95	287.5	7.44
ν_{19}	C_a-C_m (67%)	567.0	4.791	452.0	5.5			576.3	4.74
ν_{28}	C_a-C_m (52%)	498.1	4.937	494.4	4.96				

[a] Parameters from the linear-least squares fit to the data in Figure 7 (complexes E and H excluded). Slope $-K^{-1}$ (K in units of cm^{-1}/Å) and intercept A (Å) for the relation $\nu = K(A - d)$, where ν is frequency in cm^{-1} and d is the porphyrin macrocycle center-to-pyrrole nitrogen distance (Ct−N) in Å. The mode descriptions are from ref 5. [b] Parameters for metalloprotoporphyrin complexes with frequencies from solution samples and core sizes inferred largely from M(TPP) structural data. [c] Parameters for Ni-, Co-, Cu-, and Zn(OEP) complexes in CH_2Cl_2/CH_3OH solutions; core sizes adapted from ref 3. [d] Parameters for Fe^{II}(OEP) complexes of 2-MeIm and $(Im)_2$ and Fe^{III}(OEP) complexes of $(DMSO)_2$, Br^-, and $(Im)_2$ with frequencies from CH_2Cl_2 solutions and core sizes from corresponding TPP structural data, except that for the bromo complex which is referred to the structure of hemin chloride.

that for ν_{19}. We are unable to positively identify ν_{19} in [Fe(OEP)$(DMSO)_2]^+$, and in the other examples, the frequencies appear to be more scattered. In part, the identification of ν_{19} is complicated by its overlap with ν_2, when exciting within the Soret region, and with ν_{11}, when exciting within the Q-bands. For these reasons, we would use caution when calculating core-size and/or frequency with this mode. The classical oxidation-state marker ν_4 shows only a very weak dependence on the core size, hence a more vertical line, a result that has been noted previously.[13] The band ν_{28} is also sensitive to core size,[13] but because of the inherently weaker rR scattering of this mode, frequencies are probably less accurate.

The linear least-squares parameters for each of the core-size indicators from Figure 7 are listed in Table 3, together with representative K and A values from the literature. Whereas the *absolute* values of these parameters (Table 3) differ significantly, yet similar frequencies or core sizes are calculated by each of these models for a given value of d (Ct−N) or ν, respectively. Hence, there is a compensatory effect in the choices of the K and A parameters: smaller values of K are accompanied by larger values of A and vice versa. It is remarkable that previous literature values for K and A were derived largely from rR frequencies of samples of M(OEP)s or M(PPIX) in solution whereas the accompanying Ct−N values were adapted from the corresponding M(TPP)s. The parameters for OEPs and PPIXs are, thus, interchangeable, with the exception of those for ν_2, which has a different mode composition in the two sets of complexes owing to the contribution of the vinyl group frequency in the natural porphyrins.[6] The results of the present study also rationalize the previous practice of using solution rR frequencies together with crystallographic data of M(TPP)s in the derivation of core-size parameters. Interestingly, and perhaps unexpectedly, the parameters of the several data sets in Table 3 lead to very similar *frequencies* from an assumed value of Ct−N, but the deviations are much more severe in the calculation of *core size* from a set of observed frequencies. Nonetheless, this study strengthens support for using solution rR frequencies to extract structural data for less-well-studied metalloporphyrins, for example, *meso*-hydroxyhemes and verdohemes, the initial degradation products of heme oxygenase,[45] or hydroporphyrins such as cytochrome *d*, using parameters developed for M(OEC)s.[8]

It is interesting to compare the core-size marker frequencies of the four-coordinate Fe^{II}(OEP) to those of the five- and six-coordinate Fe^{III}(OEP) complexes (Table 4 and Figure 7). The frequencies of the four-coordinate ferrous complex are consistently *higher* than those of ferric Fe(OEP)(NCS) and [Fe(OEP)-$(DMSO)_2]^+$ and reflect the significantly smaller Ct−N distance in the intermediate-spin compound. Indeed, the positions of the core-size marker bands of four-coordinate Fe(OEP) are unique, being essentially identical to those of the low-spin, six-coordinate complex.

The core-size marker bands of ferrous heme proteins also appear at lower frequencies than those of Fe(OEP). These data suggest larger core sizes in the protein systems. Crystallographic data for such macrocycles are not sufficiently accurate to be included in the correlation presented here (and elsewhere) for model metalloporphyrin complexes. However, bis-ligated low-spin Fe^{II}−heme proteins also show low frequencies. Exceptions occur for HbO_2, HbNO, and HbCO, where the frequencies are close to the values for intermediate-spin Fe(OEP). For these three adducts, identification of the electronic structures of the metal/adduct complexes and, hence, the oxidation state of the iron is somewhat ambiguous.[46]

As seen in Figure 7, the plots for ν_2 and ν_{19} cross at a Ct−N value of ~1.950 Å, whereas, for systems with large core sizes of ~2.050 Å, the ν_{11} and ν_{19} bands are seen to merge. The proximity of ν_2 and ν_{19} of Fe(OEP), 1590 and 1588 cm^{-1}, respectively, relative to ν_{11} at 1563 cm^{-1} supports a smaller core size (X-ray: 1.996 Å). It should be stressed that the frequencies and core-size plot parameters for OEP complexes are very different from those of *meso*-tetraphenylporphyrins[13] and reflect the strongly altered normal mode compositions induced upon a change in the substituent pattern of the porphyrin.

Resonance Raman Spectra. Four-Coordinate Complexes. Resonance Raman spectra of Fe(OEP) and Fe(OEC) are shown in Figures 8 and 9, and the core-size sensitive bands are listed in Table 4. Infrared and resonance Raman frequencies, polarization properties, and assignments are given in Tables 5 and 6. Although these spectra show superficial similarities, the detailed spectral patterns, relative intensities, and wavelength-dependent enhancements differ. The chlorin, owing to its lower symmetry, has a larger number of rR active bands at each excitation wavelength and exhibits a rich rR spectrum with red excitation that is distinct from its porphyrin counterpart.

Fe(OEP). The most notable features of the rR spectrum of the *ferrous* porphyrin complex are the high frequencies of the marker bands.[25] Several key bands of the four-coordinate, intermediate-spin Fe(OEP) complex are as high or even higher in frequency than observed in five- and six-coordinate *ferric* complexes. The basis of this apparent anomaly is attributable to the small core size of Fe(OEP). Polarization analyses for solid samples were also carried out. Because the samples are deeply colored, meaningful polarization data may be obtained directly from the solid samples.[47] However, we noted that the depolarization ratios (ϱ) for anomalously polarized (ap) modes ($\varrho = I_\perp/I_\parallel > 0.75$) were 2× to 3× smaller for solid than solution samples.[2] Polarized bands dominate the rR spectrum of Fe-

(45) (a) Sun, J.; Wilks, A.; Ortiz de Montellano, P. R.; Loehr, T. M. *Biochemistry* **1993,** *32*, 14151. (b) Sun, J.; Loehr, T. M.; Wilks, A.; Ortiz de Montellano, P. R. *Biochemistry* **1994,** *33*, 13734. (c)Takahashi, S.; Wang, J.; Rousseau, D. L.; Ishikawa, K.; Yoshida, T.; Takeuchi, N.; Ikeda-Saito, M. *Biochemistry* **1994,** *33*, 5531.

(46) (a) Wayland, B. B.; Olson, L. W. *J. Am. Chem. Soc.* **1974,** *96*, 6037. (b) Reed, C. A.; Cheung, S. K. *Proc. Natl. Acad. Sci. U.S.A.* **1977,** *74*, 1780.

(47) Strommen, D. P.; Nakamoto, K. *Appl. Spectrosc.* **1983**, *37*, 436. Abbreviations used here are p = polarized, ap = anomalously polarized, and dp = depolarized.

Table 4. Core Sizes (Å) and Core-Size Sensitive Resonance Raman Frequencies (cm^{-1}) of Crystalline $Fe^{II,III}$(OEP) Complexes

	Fe(OEP)(NCS)	$[Fe(OEP)(N\text{-MeIm})_2]^+$ [a]	$[Fe(OEP)(DMSO)_2]^+$ [b]	Fe(OEP)	Fe(OEC)
Ct–N	2.014	2.004	2.035	1.996	1.982
ligation and spin state[c]	5cHS	6cLS	6cHS	4cIS	4cIS
mode					
ν_{10} (B_{1g})	1630	1640 dp	1609 dp	1637 dp	1628 p
ν_2 (A_{1g})	1582	1590 p	1575 p	1590 p	1577
ν_{19} (A_{2g})	1566	1588 ap	n.o.[d]	1588 ap	1589 p
ν_{11} (B_{1g})	1561	1568 dp	1556	1563 dp	1571
ν_3 (A_{1g})	1495	1505 p	1487 p	1497 p	1498 p
ν_{28} (B_{2g})	1455	1465 dp	1444	1466 dp	1460
ν_4 (A_{1g})	1374	1376 p	1376 p	1375 p	1370 p

[a] Polarization measured in CH_2Cl_2 solution to which ~500 mM *N*-MeIm had been added. [b] Polarization measured in 1:1 CH_2Cl_2–DMSO solution. [c] c = coordinate, H = high, I = intermediate, L = low, S = spin. [d] n.o. = not observed.

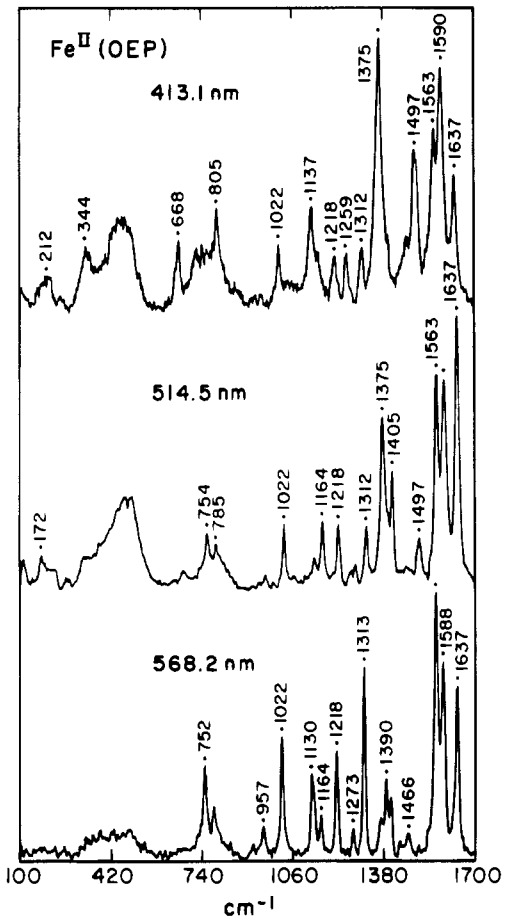

Figure 8. Resonance Raman spectra of microcrystalline Fe(OEP) sealed in a glass capillary tube, placed in a cold finger immersed in an ice-water mixture, and excited at 413.1, 514.5, and 568.2 nm, respectively. The scattered light was collected in a backscattering geometry. Typical data collection conditions were as follows: laser power at the sample, ~20 mW (413.1 nm) and ~40 mW (longer wavelengths); scan rate, 1 cm^{-1}/s; spectral resolution, 4–8 cm^{-1}; signal averaging by multiple accumulations of 4–16 scans. The broad feature from ~350–550 cm^{-1} is Raman scattering from the glass capillary. Background correction and Savitzky–Golay smoothing applied to the data. Polarization data listed in the tables were obtained from solution samples in flame-sealed NMR tubes dissolved in C_6H_6 and C_6D_6.

(OEP) obtained with B excitation as has been observed for other metalloporphyrins, whereas ap and dp modes dominate in spectra obtained with Q excitation.

The oxidation-state marker band, ν_4, of Fe(OEP) at 1375 cm^{-1} is most intense with B-band excitation, as expected, but it is essentially absent in the 568.2-nm spectrum (Figure 8). For comparison, ν_4 occurs at 1373–1378 cm^{-1} in axially ligated high- and low-spin Fe^{III}porphyrin complexes (see Figures 10–12, below) and a typical value for axially ligated Fe^{II} complexes

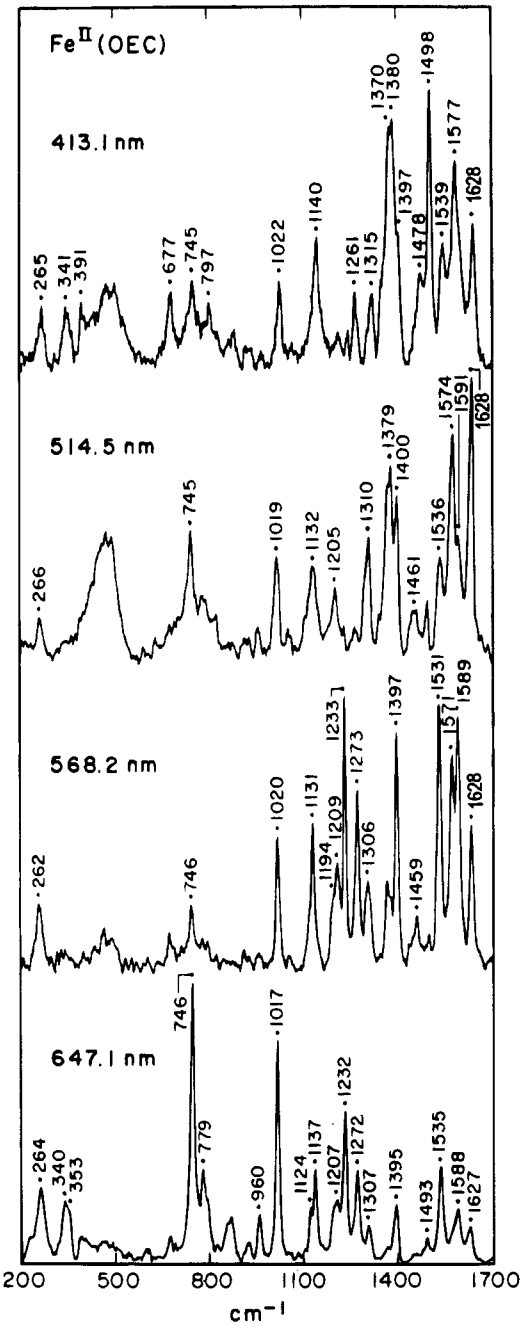

Figure 9. Resonance Raman spectra of microcrystalline Fe(OEC) sealed in a glass capillary tube cooled to ~2 °C and excited at 413.1, 514.5, 568.2, and 647.1 nm, respectively. Typical data-collection parameters are given in the legend to Figure 8.

is ~1360 cm^{-1}. The position of ν_4 at 1375 cm^{-1} in spectra of four-coordinate Fe(OEP) is, therefore, unique relative to high-

and low-spin, axially coordinated Fe^{II} systems but closely matches the ν_4 position of other intermediate-spin, four-coordinate metalloporphyrin complexes.[25]

Four C_a-C_m and two C_b-C_b stretching vibrations are Raman allowed for Fe(OEP). Resonance Raman bands at 1637 (dp), 1588 (ap), and 1497 (p) cm^{-1} are assigned to modes involving mainly C_a-C_m stretching vibrations (ν_{10}, ν_{19}, and ν_3, respectively). Bands at 1590 (p) and 1563 (dp) cm^{-1} have significant C_b-C_b stretching character (ν_2 and ν_{11}, respectively).[48,49] The λ_{max}[Q(0,0)] of Fe(OEP) is close to 568 nm. The rR features show large changes at this excitation wavelength as compared with B-band excitation. Thus, ν_3 is only significantly enhanced at the latter wavelength. The ap bands can be seen clearly at 1588 (ν_{19}), 1390 (ν_{20}), 1313 (ν_{21}), and 1130 (ν_{22}) cm^{-1} with visible excitation and careful polarization measurements. Although the ν_2 and ν_{19} bands are very close in frequency (± 2 cm^{-1}), these bands are distinguishable because of their different polarization properties (as observed with 514.5-nm excitation; data not shown). The appearance of rR bands in both B- and Q-band spectra indicates that their normal modes contribute to both vibronic and Franck–Condon scattering mechanisms.[50,51] One notable example is the Fe(OEP) ethyl mode at 1022 cm^{-1} that exhibits moderate intensity at all excitations. The ap modes $\nu_{20}-\nu_{22}$ are most clearly seen with Q-band excitations but are still apparent with Soret excitation and, thus, also indicate Q–B vibronic mixing.

The low-frequency modes of Fe(OEP) are more distinct with 413.1-nm excitation than with other wavelengths, as is typical of other porphyrins.[52] The bands at 138 (not shown) and 343 cm^{-1} are assigned to ν_{35} and ν_8, respectively. These values are in agreement with those of Ni(OEP).[48] The symmetric pyrrole deformation mode ν_7 at 668 cm^{-1} and pyrrole breathing mode ν_6 at 805 cm^{-1} are intense with B-band excitation but are weak with Q_y excitation. The weak bands at 785, 921, and 957 cm^{-1} in Q_y excitation are assigned to CH_2 rocking, ν_{32}, and $\delta(CH_3)$, respectively, and are very weak in Soret spectra.

Fe(OEC). The rR frequency positions for four-coordinate, $S = 1$, Fe(OEC) are higher than typical for an Fe^{II} chlorin system (Figure 9). Owing to the low site symmetry of Fe(OEC), eight C_a-C_m (4A + 4B) and four C_b-C_b (2A + 2B) are Raman allowed. These bands appear very close together and can be separated by polarization measurements (data not shown) and different excitation wavelengths. Overlapping bands are seen in the oxidation-state-marker region (ν_4 of metalloporphyrins), a diagnostic feature of chlorin rR spectra.[10-12] These bands are most intense for Fe(OEC) with B excitation and change their relative intensities with longer wavelength excitation. However, the presence of multiple bands in this region is clearest in the 514.5-nm spectrum. Another characteristic property of chlorin systems that is distinct from the higher symmetry porphyrin macrocycles is their pronounced rR enhancement upon excitation within their long wavelength $Q_y(0,0)$ absorption band. The 647.1-nm spectrum of Fe(OEC) shown in Figure 9 is a nice illustration of this point; Fe(OEP) and other metalloporphyrins are not enhanced at this wavelength.

Many chlorin bands also show selective enhancement. For example, intense bands observed at ~1233, 1273, and 1531 cm^{-1} with 568.2-nm excitation show little or no enhancement in the 514.5-nm spectrum and are also significantly diminished with red excitation (Figure 9). The bands at 746 and 1017 cm^{-1} are the most intense observed with $Q_y(0,0)$ excitation. The former corresponds to macrocyclic deformation because its intensity appears to correlate well with ruffled macrocycles[53] and has been suggested to be a chlorin-ring stereochemistry marker.[10e] The corresponding band in Fe(OEP), ν_{16}, does not show comparable intensity changes with excitation wavelength. The band at ~1020 cm^{-1} in spectra of Fe(OEC) is also enhanced with red excitation. As with porphyrin and even isobacteriochlorin systems, this band appears to be present only in octaethyl-substituted tetrapyrrole macrocycles.[11,54]

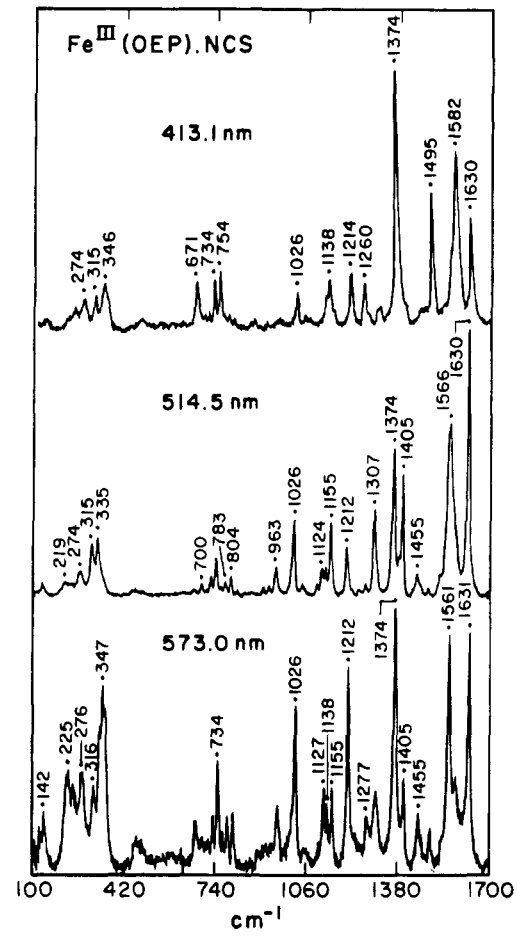

Figure 10. Resonance Raman spectra of microcrystalline Fe(OEP)(NCS) obtained from a spinning sample at room temperature. A weighed amount of solid sample was diluted in 1:200 (w/w) spectral-grade KBr and mixed by gentle grinding in an agate mortar, and the powder mixture was packed lightly into a 1-mm deep groove of a stainless-steel spinning-sample holder. Spectra were obtained in a backscattering geometry by illumination of the groove with a slit-shaped beam. The sample holder is rotated at ~1000 rpm to reduce thermal degradation by the laser. Similar data were obtained when a static arrangement was used. For both cases, typical data-collection parameters are given in the legend to Figure 8. The 573-nm line was generated by the dye laser.

Five- and Six-Coordinate Ferric Complexes. Resonance Raman spectra of the high-spin five-coordinate ferric complex Fe(OEP)(NCS) at different excitation wavelengths are shown in Figure 10, and the high-frequency regions (only) of the two new six-coordinate complexes are shown in Figures 11 and 12.

(48) Li, X.-Y.; Czernuszewicz, R. S.; Kincaid, J. R.; Stein, P.; Spiro, T. G. *J. Phys. Chem.* **1990**, *94*, 47.
(49) Abe, M.; Kitagawa, T.; Kyogoku, Y. *J. Chem. Phys.* **1978**, *69*, 4526.
(50) Spiro, T. G.; Stein, P. *Annu. Rev. Phys. Chem.* **1977**, *28*, 501.
(51) Tang, J.; Albrecht, A. C. In *Raman Spectroscopy*; Szymanski, H. A., Ed.; Plenum Press: New York, 1970; Vol. 2, p 33.
(52) Spiro, T. G. In *Iron Porphyrins*; Lever, A. B. P., Gray, H. B., Eds.; Addison-Wesley: Reading, MA, 1983; Part II, Chapter 3.
(53) Andersson, L. A.; Loehr, T. M.; Cotton, T. M.; Simpson, D. J.; Smith, K. M. *Biochim. Biophys. Acta* **1989**, *974*, 163.
(54) (a) Han, S.; Madden, J. F.; Thompson, R. G.; Strauss, S. H.; Siegel, L. M.; Spiro, T. G. *Biochemistry* **1989**, *28*, 5461. (b) Melamed, D.; Sullivan, E. P., Jr.; Prendergast, K.; Strauss, S. H.; Spiro, T. G. *Inorg. Chem.* **1991**, *30*, 1308.

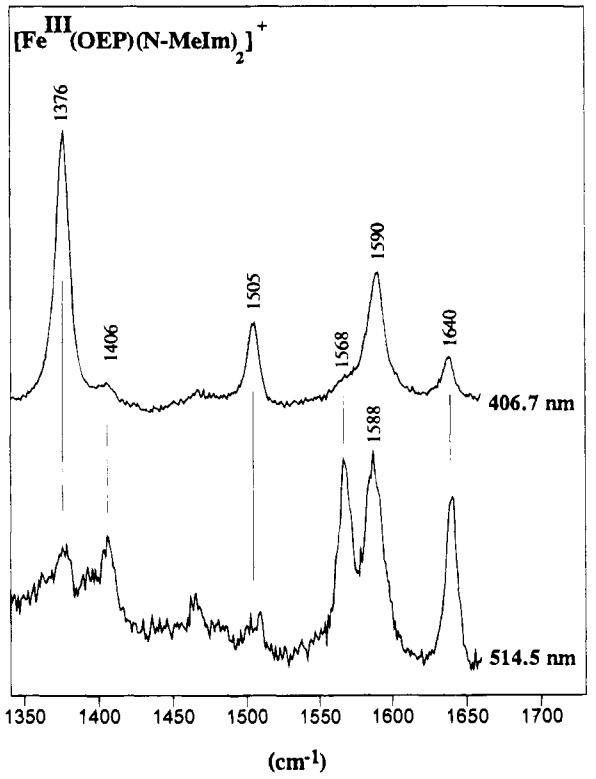

Figure 11. Resonance Raman spectra of [Fe(OEP)(*N*-MeIm)$_2$][Ag(*N*-MeIm)$_2$][PF$_6$]$_2$ in the high-frequency region. The sample was prepared by diluting the microcrystalline specimen with 1−3% Na_2SO_4 by weight. Other conditions paralleled those given under Figures 10 and 8, with the exception that the data are shown as collected. Polarization data reported in Table 4 were obtained from a CH_2Cl_2 solution to which 500 mM free *N*-methylimidazole was added.

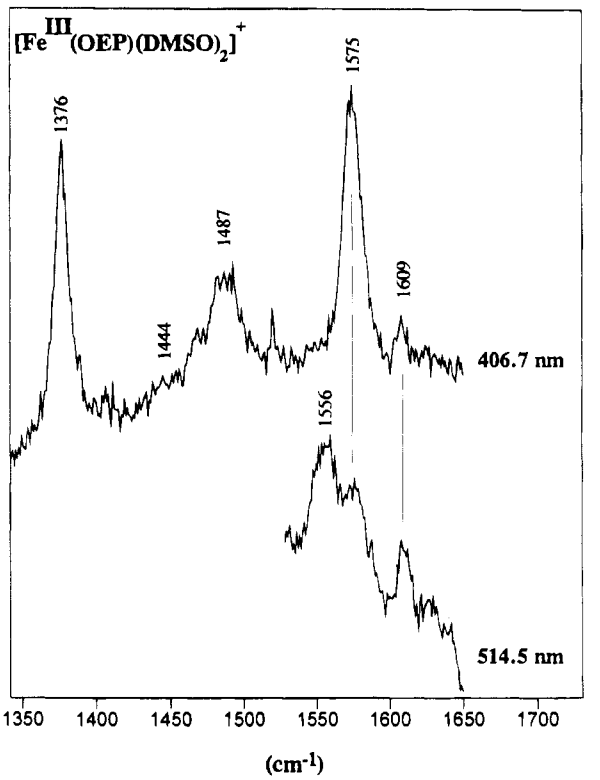

Figure 12. Resonance Raman spectra of [Fe(OEP)(DMSO)$_2$][PF$_6$] in the high-frequency region obtained with 406.7- and 514.5-nm excitation and prepared as described in the legend to Figure 11. Polarization data reported in Table 4 were obtained from a 1:1 CH_2Cl_2:DMSO solution. Data are shown as collected.

Spectral assignments for the core-size sensitive indicator bands of these Fe^{III}(OEP) complexes are given in Table 4 and are based on excitation wavelength dependence, polarization data, and reference to similar rR data in the literature for high-spin Fe^{III} complexes, as well as core-size correlation data.[3,6,8,13,15,52]

Fe(OEP)(NCS). The bands ν_2, ν_3, and ν_4 are intense and polarized in Soret excitation spectra and are seen at 1582, 1495, and 1374 cm^{-1}, respectively. The 1630-cm^{-1} band is ν_{10}; it is already well apparent with Soret excitation, and it becomes the dominant band with Q excitation. The overall spectrum is very similar to that of the analogous complex, Fe(OEP)Br.[8] The Fe^{III}−(NCS) axial ligand stretching mode was previously assigned by Ogoshi et al.[20] and is observed at ~315 cm^{-1}. With Q-band excitation, the most significant spectral changes occur in the high-frequency region, as expected, to allow ν_{19} (1566 cm^{-1}) and ν_{28} (1455 cm^{-1}) to be observed. The prominent band at 1405 cm^{-1} in the 514.5-nm spectrum is ν_{29}. With still longer wavelength excitation, the asymmetric band at ~1566 cm^{-1} (composed of ν_2 and ν_{19}) sharpens to reveal a new maximum at 1561 cm^{-1} that we assign to ν_{11}.

[Fe(OEP)(*N*-MeIm)$_2$]$^+$. Crystals of the low-spin six-coordinate complex show prominent bands for ν_2, ν_3, and ν_4 at 1590, 1505, and 1376 cm^{-1} with Soret excitation (Figure 11, Table 4). The highest frequency band at 1640 cm^{-1} is ν_{10}, and its position is indicative of the low-spin nature of the compound with two strong axial ligands. As the excitation wavelength is increased to 514.5 nm, the strongly polarized A_{1g} modes diminish and new bands appear at 1568 (ν_{11}) and 1588 cm^{-1} (ν_{19}). Although ν_2 and ν_{19} differ by only 2 cm^{-1}, the close accidental degeneracy can be resolved by studies of their degree of depolarization (data not shown). Although the 1590-cm^{-1} peak is polarized in the 406.7-nm spectrum, its ρ value is higher than those for ν_3 and ν_4 (both p) owing to the underlying contribution of the residual ν_{19}. On the other hand, the 1588-cm^{-1} band in the Q-band excited rR spectrum, although not markedly ap, has a ρ value higher than those for ν_{10} and ν_{11} bands (both dp), owing to the underlying residual contribution of ν_2. The weak features at 1406 and 1465 cm^{-1} are in the expected positions for ν_{29} and ν_{28}, respectively. Overall spectral properties are similar to those reported for methylene chloride solutions of [Fe(OEP)(Im)$_2$]$^+$ by Ozaki et al.[8]

[Fe(OEP)(DMSO)$_2$]$^+$. The high-frequency rR spectrum of the crystalline, six-coordinate (DMSO)$_2$ complex is shown in Figure 12, and its frequencies are given in Table 4. Frequencies for solution samples of this system have been reported previously with similar results.[5,8] The Soret-excited rR spectrum shows equally intense bands at 1376 and 1575 cm^{-1} for ν_4 and ν_2, respectively, a weak ν_3 at 1487 cm^{-1}, and only a very minor band at ~1610 cm^{-1} corresponding to ν_{10}. The latter is more pronounced with longer wavelength excitations. Because low laser power had to be used to prevent photodegradation in the crystalline state, only a small region of the spectrum is shown in Figure 12, where it is seen that ν_2 diminishes in intensity and a new band appears at 1556 cm^{-1}. We ascribe this peak to ν_{11} on the basis that the core-size correlation in Figure 7 is more satisfactory, although this feature may be admixed or even coincident with ν_{19}. At this wavelength, the 1609-cm^{-1} band of ν_{10} is more prominent. At higher laser power (data not shown), a 1632-cm^{-1} band grows in that is characteristic of ν_{10} of a five-coordinate ferric porphyrin (1630 cm^{-1} in Fe(OEP)(NCS)) and probably represents loss of one DMSO ligand. Similarly, rR spectra obtained at 496.5 nm in a dilute (50 μM DMSO in CH_2Cl_2) solution show a 1632-cm^{-1} peak, but this peak is absent in a spectrum obtained under identical conditions with a 1:1 (v/v) solution mixture. Finally, a very weak feature at 1444 cm^{-1} is in the correct position for ν_{28}.

Table 5. Resonance Raman and Infrared Frequencies and Tentative Assignments for Fe(OEP)[a]

resonance Raman				Infrared
ν, cm^{-1}	mode	ϱ[b]	assignment	ν, cm^{-1}
1637	ν_{10}	dp	B_{1g}	1664 m, b
1590	ν_2	p	A_{1g}	1462
1588	ν_{19}	ap	A_{2g}	1450
1563	ν_{11}	dp	B_{1g}	1383
1497	ν_3	p	A_{1g}	1375
1466	ν_{28}	dp	B_{2g}	1367
1405	ν_{29}	dp	B_{2g}	1313 m
1390	ν_{20}	ap	A_{2g}	1305 m
1375	ν_4	p	A_{1g}	1266 s
1313	ν_{21}	ap	A_{2g}	1221 m
1273	CH_2 twist			1180 w
1259	$\nu_5 + \nu_9$	p	A_{1g}	1165 m
1218	ν_{13}	ap	B_{1g}	1145 s
1164	ν_{30}	dp	B_{2g}	1109 m
1137	ν_5	p	A_{1g}	1076 w
1130	ν_{22}	ap	A_{2g}	1062 m
1022	νC_1-C_2 (Et)	p	A_{1g}	1054 s
957	γCH_3	p	A_{1g}	1015 s
925	ν_{32}			984 m
841	oop			955 s
805	ν_6	p	A_{1g}	918 m
785	CH_2 rock			891 w
753	ν_{15}	dp	B_{1g}	844 m
720	oop			836 s
668	ν_7	p	A_{1g}	829 s
344	ν_8	p	A_{1g}	773 w
				747 m
				732 s
				722 s
				699 m
				499 m, b

[a] Table entries are average values from repeat experiments and multiple excitation wavelengths. [b] p = polarized, ap = anomalously polarized, dp = depolarized, oop = out-of-plane porphyrin-ring deformation mode.

Conclusions. The present study reports the crystal structures of three new Fe^{III}(OEP) complexes: the pentacoordinate, high-spin Fe(OEP)(NCS)·$C_6H_5CH_3$, the hexacoordinate, low-spin $[Fe(OEP)(N\text{-MeIm})_2]^+$ isolated as $[Fe(OEP)(N\text{-MeIm})_2][Ag(N\text{-MeIm})_2][PF_6]$, and the high-spin, hexacoordinate $[Fe(OEP)(DMSO)_2][PF_6]$. In addition, we review the structural properties of two tetracoordinate, intermediate-spin ($S = 1$) complexes, Fe(OEP) and Fe(OEC). Resonance Raman spectra have been obtained for these complexes at different excitation wavelengths. Complete spectra (rR spectra and tables of rR and FTIR frequencies) are reported for the four-coordinate porphyrin and chlorin compounds. Complete spectra are also presented for Fe(OEP)(NCS). For the hexacoordinate Fe^{III}(OEP) complexes, only spectral data in the 1350−1700-cm^{-1} range are reported; this region of the rR spectrum contains the most reliable core-size marker bands that are the focus of this study. Analysis of the present data permits the first rigorous test of earlier Ct−N vs frequency correlations in that the spectroscopic and structural parameters are taken from the *same* compounds in the *same* crystalline phase. As found in previous studies, the rR frequencies of core-size sensitive porphyrin modes (ν_2, ν_3, ν_{10}, ν_{11}, ν_{19}, and ν_{28}) have inverse linear dependence on Ct−N values: $\nu_i = K_i(A_i - d)$. The exact values of the parameters K_i and A_i differ from the corresponding OEP values in previous studies that were obtained from both solid and solution rR frequencies of OEP and PPIX compounds but from Ct−N values of *meso*-tetraphenyl-substituted metalloporphyrin crystal structures. The present rR data for these *crystallographically characterized complexes* yield a new core-size correlation for β-pyrrole-substituted metalloporphyrins. With the present analysis as a foundation, rR spectroscopic studies may be extended to simple complexes in solution as well as heme proteins in the determination of core sizes and in facilitating spectral assignments.

Table 6. Resonance Raman and Infrared Frequencies and Partial Assignments for Fe(OEC)[a]

resonance Raman				
ν, cm^{-1}	porphyrin-equiv mode	ϱ[b]	sym	infrared ν, cm^{-1}
1628	ν_{10}	p	A	1689 w
1594				1628 s
1577	ν_2	p	A	1598 m
1589	ν_{19}	ap	B	1575 m
1571	ν_{11}			1539 m
1539	ν_{38}	p	A	1456 s
1531		p	A	1385 w, sh
1498	ν_3	p	A	1376 m
1478		ap	B	1366 m, sh
1460	ν_{28}		B	1312 m
1398	ν_{29}	dp	B	1268 s, sh
1380	ν_{20}	dp	B	1262 s
1370	ν_4	p	A	1223 w
1367		ap	B	1200 s
1315				1184 m
1308		ap	B	1169 w
1273		p	A	1145 m
1261		p	A	1122 m
1232		p	A	1107 m, b
1205		p	A	1054 s
1194		p	A	1015 s
1147		dp	B	990 m
1140		p	A	958 s
1124		ap	B	919 m
1058		dp	B	889 w
1022		p	A	847 s
1018		ap	B	832 s
960		p	A	808 s, b
925		p	A	746 m
871				729 s
859				704 m
824				677 m
795		p	A	598 w
779		dp	B	
746				
677				
391				
353		p	A	
340				
264	ν_9			

[a] Table entries are average values from repeat experiments and multiple excitation wavelengths. [b] p = polarized, ap = anomalously polarized, dp = depolarized.

Acknowledgment. We gratefully acknowledge the following support for this research: the National Institutes of Health, Grant GM 34468 (T.M.L. and L.A.A); the National Science Foundation, Grant CHE-8805788 (S.H.S.); the donors of the Petroleum Research Fund, administered by the American Chemical Society, Grant PRF 19653-AC3 (S.H.S.). The CSU Siemens *R3m* diffractometer and computing system were purchased with funds from NSF Grants CHE-8103011 and CHE-9107593. Instrumentation at the OGI Shared Raman Spectroscopy Facility was made possible by NIH Grant S10 RR02676.

Supporting Information Available: Complete tables of atomic coordinates, and U values, bond distances and angles, and anisotropic thermal parameters for Fe(OEP)(NCS)·C_7H_8, $[Fe(OEP)(N\text{-MeIm})_2][Ag(N\text{-MeIm})_2][PF_6]_2$, and $[Fe(OEP)(DMSO)_2][PF_6]$ (16 pages). This material is contained in many libraries on microfiche, immediately follows this article in the microfilm version of the journal, and can be ordered from the ACS; see any current masthead page for ordering information.

IC950064O